

Michael Fleck^a, Efim A. Brener^a, Robert Spatschek^b, Bernhard Eidel^b

^aInstitute for Solid-State Research, Forschungszentrum Jülich, Jülich, Germany

^bInterdisciplinary Centre for Advanced Materials Simulation (ICAMS), Ruhr-Universität Bochum, Germany

Elastic and plastic effects on solid-state transformations: A phase field study

We discuss a model of diffusion limited growth in solid-state transformations, which are strongly influenced by elastic effects. Density differences and structural transformations provoke stresses at interfaces, which affect the phase equilibrium conditions. We study the growth of a stable phase from a metastable solid in a channel geometry, and perform phase field simulations. Extensions to plastic models are discussed.

Keywords: Dendritic growth; Elastic effects; Solid-state transformations; Plasticity

1. Introduction

Transformations between different solid states of a material are essential for many technological and scientific applications, and understanding their kinetics is therefore not only interesting because of the scientific variety and beauty, but also important for tailoring new materials with specific properties. During these transformation processes, density differences or structural changes between the solid phases often provoke elastic or plastic deformations in the bulk and at the interfaces [1, 2].

There are many important analogies between solidification and diffusion-limited solid-state transformation, and a recent review on similarities is given in [3]. These similarities include the growth of needles and plates similar to Ivantsov paraboloids, i.e. dendrites versus Widmanstätten structures, coupled growth of eutectics and eutectoids, and massive transformations. From microscopic solvability theory of solidification it is known that the questions concerning existence, shape and growth velocity of steady state patterns in solidification crucially depend on selection mechanisms. In this spirit the influence of many different physical effects on solidification or melting processes has been studied throughout the years [4, 5]. For example, the effect of isotropic surface tension was proven not to serve as a selection mechanism for a solution in free space, whereas anisotropic surface tension leads to a unique solution. On the other hand, steady state dendrite-like growth is even possible without anisotropy of surface tension due to elastic effects, in contrast to diffusion-limited solidification [6]. In the present work we therefore focus on the role of elastic and plastic effects on the kinetics of diffusion-limited solid-state transformations; surface anisotropy effects are therefore excluded intentionally.

Phase field methods have emerged as a powerful tool to investigate solidification and also solid-state transformations; for a general overview see e.g. [7–9]. In contrast to,

for instance, qualitative phase field investigations for complex transitions in Ti–Al–Nb [10–13] and generic two-dimensional dendritic structures in [14], we investigated the role of selection principles in [15, 16] with sharp interface and phase field methods. In the present paper, we concentrate on predictions from phase field simulations under the influence of elastic effects; in the end, we show first results demonstrating the incorporation and relevance of plasticity.

2. Diffusion-limited solid-state transformations

Despite the relationship of phase field models to sharp interface descriptions, we describe the latter only very briefly. For details, we refer to [15, 16].

Specifically, we consider a non-equilibrium system consisting of two solid phases below the bulk equilibrium temperature T_{eq} . The thermodynamically favorable phase β grows at the expense of the high temperature phase α . In contrast to massive transformations that have been studied e.g. in [17], we assume here that the process is limited by diffusion; that is, at the interface between α and β either latent heat L is absorbed or emitted and has to be transported away, or the partitioning of solute leads to diffusion, which – in both cases – is assumed to be rate limiting. For the sake of clarity, we formulate the problem here in terms of heat diffusion. In both solid phases, the temperature therefore obeys a diffusion equation; here we discuss only symmetrical situations with equal heat diffusivity. The front velocity at each interface point is then directly proportional to the difference of heat fluxes into the interface. The temperature itself obeys a local equilibrium condition at the interface. Up to this point, there is no difference between the modeling of solid-state transformations and for example dendritic growth during solidification. The difference is now that density and structural differences between the coherently connected solid phases provoke elastic stresses, and they modify the equilibrium temperature. This can be analyzed in the framework of sharp interface descriptions [2, 15, 16, 18] and emerges naturally from phase field descriptions; extensions toward plastic effects are much more straightforward in such an approach. The elastic degrees of freedom relax quickly on diffusive timescales, and therefore the application of static elasticity is legitimate.

It turns out that the precise nature of the transition is very important; it is here reflected by the transformation or stress-free strain ε_{ik}^0 . Taking the α phase as reference, a relaxed β phase can differ from it both in shape and volume. In the case of a density change only, the eigenstrain tensor is proportional to the unit matrix, $\varepsilon_{ik}^0 = \varepsilon \delta_{ik}$. Another example are hexagonal to orthorhombic transformations, which

occur for example in Ti–Al–Nb systems [10–13]. Here, the volume of the unit cell is conserved and only the shape is changed, which is reflected by a traceless eigenstrain tensor. Of course, mixtures of these two extreme cases are also possible, and for a discussion we refer to [15, 16].

For the formulation of a phase field model, we first introduce the order parameter φ , having the value $\varphi = 1$ in the initial α phase and the value $\varphi = 0$ in the β phase. The two phases are separated by a smooth interface-region of width ξ , where the phase field variable changes continuously between its bulk values, $\varphi = 0, 1$. We start from a free energy functional,

$$F[\varphi, u_i, T] = \int_V (f_s + f_{dw} + f_{th} + f_{el}) dV \quad (1)$$

where $f_s(\nabla\varphi) = 3\gamma\xi(\nabla\varphi)^2/2$ is the gradient energy density and $f_{dw}(\varphi) = 6\gamma\varphi^2(1-\varphi)^2/\xi$ is the double well potential, guaranteeing that the free energy functional has two local minima at $\varphi = 0$ and $\varphi = 1$ corresponding to the two distinct phases of the system. The form of the double well potential and the gradient energy density are chosen such that the phase field parameter ξ defines the interface width and γ corresponds to the interface energy [19]. The thermal contribution to the free energy, $f_{th}(\varphi, T)$, is proportional to the temperature deviation from thermal equilibrium,

$$f_{th} = L \frac{T - T_{eq}}{T_{eq}} h(\varphi) \quad (2)$$

where the interpolation function h is chosen to be $h(\varphi) = 1 - \varphi^2(3 - 2\varphi)$. The elastic contribution to the free energy density f_{el} depends on the displacement u_i and is given by

$$f_{el} = \frac{E}{2(1+\nu)} \left(\frac{\nu}{1-2\nu} (\varepsilon_{ii} - h(\varphi)\varepsilon_{ii}^0)^2 + (\varepsilon_{ik} - h(\varphi)\varepsilon_{ik}^0)^2 \right) \quad (3)$$

and contains the transformation strain ε_{ik}^0 in the β phase, Young's modulus E , Poisson ratio ν and the strain tensor $\varepsilon_{ik} = (\partial_i u_k + \partial_k u_i)/2$. We use the sum convention for repeated indices, e. g. $\varepsilon_{ii} = (\varepsilon_{xx} + \varepsilon_{yy} + \varepsilon_{zz})$. Furthermore, we assume here that the elastic constants are equal in both phases.

The evolution equation of the phase field is given by the variational expression

$$\frac{\partial\varphi}{\partial t} = -\frac{M}{3\gamma\xi} \left(\frac{\delta F}{\delta\varphi} \right)_{u_i, T} \quad (4)$$

Mechanical equilibrium demands $\partial\sigma_{ik}/\partial x_k = -\delta F/\delta u_i = 0$. For the temperature field we have the usual thermal diffusion equation, with the motion of the phase field or interface being a source of latent heat,

$$\frac{\partial T}{\partial t} = D\nabla^2 T + \frac{L}{C} h'(\varphi) \frac{\partial\varphi}{\partial t} \quad (5)$$

with the thermal diffusivity D , the heat capacity C and the latent heat L , as mentioned above. The phase field model presented here is very similar to the model in [20].

3. Applications

As a specific application, we consider here a case that involves shear strain, where velocity selection is possible

even in free dendrite-like growth [15]: $\varepsilon_{xx}^0 = 0$, $\varepsilon_{yy}^0 = \varepsilon$, $\varepsilon_{zz}^0 = \varepsilon/2$, and all other components vanish. Since this infinitesimal strain tensor is not invariant under rotations, we can therefore expect to find directions that are more favorable for growth; for the first application for growth in a channel, we therefore align the direction of the strip with this fastest propagation direction. This situation is depicted in Fig. 1, where the thermodynamically stable β phase grows at the expense of the metastable α phase in a finite channel of width W .

The system is assumed to be effectively two-dimensional by translational invariance in the z -direction, and the α phase far in front of the growing tip is set to be at the undercooling temperature T_∞ ; from a mechanical point of view, the material is fully relaxed there.

Furthermore, we discuss three different types of boundary conditions for temperature and the elastic fields at the channel walls, which all allow for phase coexistence in a finite range of undercooling. The first variant corresponds to a thermally insulated and elastically confined channel, where we choose fixed grip boundary conditions for the displacement, i. e. $u_x \equiv 0$ and $u_y \equiv 0$, in combination with thermal insulation, $\partial T/\partial y = 0$, for the temperature field; we abbreviate this case by FG. As second variant, we consider isothermal channel walls with fixed displacements (denoted by ISO), and as the third variant again a thermally insulating but now infinitely compliant channel, where no stresses act on the walls (SF). From a physical point of view, the choice of boundary conditions is crucial in many respects, especially if the new β phase fills the channel almost completely. Due to the eigenstrain of the transformation, the material is deformed, and depending on the mechanical boundary conditions we therefore expect different deformation states, which influence the growth kinetics. Similarly, the temperature field has a nontrivial behavior even in the case of boundaries with a fixed temperature, since the moving boundaries act as heat sources due to the entropy difference between the α and the β phases. For the phase field we use wetting conditions at the upper and lower boundaries ($\varphi = 1$), therefore there is always an interface present in the tail region.

Far behind the tip, the system can reach a heterogeneous two-phase state with (asymptotically) constant temperature and zero interface velocity. Here, for all three variants of boundary conditions the volume fraction λ of the new phase

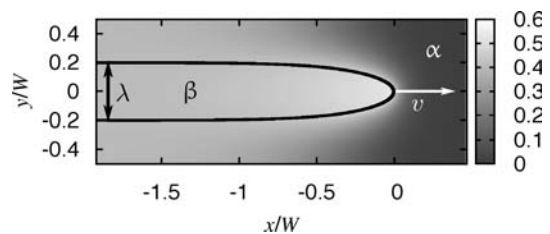


Fig. 1. Geometrical setup of a Single crystal of an equilibrium solid phase β , growing with the steady state velocity v in a finite Channel of width W . The Interface contour (denoted by the bold solid line) and the temperature field (illustrated by the gray-scaling) are obtained by a phase field simulation, and the parameters for the considered case are $\Delta_{s1} = 0.05$, $\Delta = 11/15$ and $\nu = 1/3$. Asymptotically far behind the tip, where the interface becomes straight, the Simulation confirms the asymptotic fraction of new phase as $\lambda_{sim} = 0.401$, and the average tail temperature can be measured as $C(T_\infty - T_{-})/L = 0.4$, which agrees with the theoretical prediction. The thickness of the interface contour is the phase field interface width, which is chosen to be $\xi/W = 0.0125$.

can be calculated analytically. In the cases with thermal insulation also the temperature in the tail region has to be found self-consistently, because in these cases the release of the latent heat causes the tail temperature $T_{-\infty}$ to be higher than the undercooling temperature T_{∞} ahead of the tip. There we find from heat conservation

$$T_{-\infty} = T_{\infty} + \lambda \frac{L}{C} \quad (6)$$

To obtain an analytical expression for the asymptotic phase fraction λ , we have to calculate the energy excess, which is the difference between the free energy far in front and far behind the tip. It depends on the thermal and elastic boundary conditions at the channel walls, and we obtain for fixed grip boundary conditions and thermal insulation (FG)

$$\delta\mathcal{F}(\lambda) = \frac{WL^2}{CT_{\text{eq}}} \left((\Delta - \Delta_{\text{el}}) \lambda - \frac{1}{2} (1 + a_{\text{el}} \Delta_{\text{el}}) \lambda^2 - \frac{2d_0}{W} \right) \quad (7)$$

where $a_{\text{el}} = 2(2 - \nu)^2 / (1 - 2\nu)$ is a parameter accounting for the type of eigenstrain, $\Delta_{\text{el}} = CT_{\text{eq}} E \varepsilon^2 / [8L^2(1 - \nu^2)]$ is the elastic hysteresis shift, which is a measure for the strength of elastic effects, and d_0 the capillary length (for details see [15]). The above expression differs from the case of thermal insulation and stress free boundaries (SF) only by the term $a_{\text{el}} \Delta_{\text{el}} \lambda^2$, which is not present in the latter case, since the material can expand freely perpendicular to the growth direction, see [16]. Finally, for the case of fixed displacements but isothermal channel walls (ISO, the temperature is everywhere equal to T_{∞} on the boundaries), the other term which is quadratic in the fraction λ does not appear, see [17].

Thermodynamic equilibrium asymptotically far behind the tip demands maximization of the energy excess, $\partial\delta\mathcal{F}(\lambda)/\partial\lambda = 0$, which provides an expression for the fraction of new phase β for clamped and thermally insulating boundaries

$$\lambda^{[\text{FG}]}(\tilde{\Delta}) = \frac{\tilde{\Delta}}{1 + a_{\text{el}} \Delta_{\text{el}}} \quad (8)$$

where $\tilde{\Delta} = \Delta - \Delta_{\text{el}}$ is the dimensionless driving force. Apart from this maximization condition, growth of the β phase requires also the free energy excess to be positive, $\delta\mathcal{F}(\tilde{\Delta}) \geq 0$. This is equivalent to the condition $\tilde{\Delta} > \tilde{\Delta}_{\text{crit}}$, where $\tilde{\Delta}_{\text{crit}}$ is given by

$$\tilde{\Delta}_{\text{crit}}^{[\text{FG}]} = \sqrt{\frac{4d_0}{W} (1 + a_{\text{el}} \Delta_{\text{el}})} \quad (9)$$

Hence, for a driving force above the critical value, $\tilde{\Delta} > \tilde{\Delta}_{\text{crit}}$, and for $\lambda(\tilde{\Delta}) < 1$ according to Eq. (8), we obtain coexisting α and β phases in the tail region.

For comparison, in the case of thermal insulation and stress free boundaries (SF), the fraction and the driving force are equal, $\lambda^{[\text{SF}]} = \tilde{\Delta}$, and we obtain for the critical driving force $\tilde{\Delta}_{\text{crit}}^{[\text{SF}]} = \sqrt{4d_0/W}$ [16]. Finally, for isothermally undercooled and clamped channel walls (ISO), the expression for the fraction of the new phase and the critical driving force become $\lambda^{[\text{ISO}]} = \tilde{\Delta} / a_{\text{el}} \Delta_{\text{el}}$ and $\tilde{\Delta}_{\text{crit}}^{[\text{ISO}]} = \sqrt{4a_{\text{el}} d_0 \Delta_{\text{el}} / W}$.

The steady state interface shape and temperature distribution of a single crystal of a growing β phase in a thermally insulating and elastically confined channel (FG) is shown in Fig. 1. We point out that the tip radius is neither determined by the channel width W nor the interface thick-

ness ξ , and instead independent selection principles become relevant here [15].

For the three different types of boundary conditions, we performed a series of phase field simulations with different driving forces, and the results are shown in Fig. 2. In each case we start with a small seed of the β phase surrounded by the undercooled metastable α phase, and follow the growth of β phase. Although the channel is regarded to be infinitely extended in the lateral direction, the simulations were restricted to a finite domain around the right tip of the β phase, to reduce the computational efforts. Hence we shift all fields when the tip has progressed too far. Obviously, the steady state velocity grows with increasing driving force, and the three curves corresponding to the different boundary conditions are close to each other. The limit of vanishing velocity is in agreement with the analytical prediction (9) and the corresponding conditions for the other types of boundaries. The discrepancies between the curves are related to the finite channel width; it is intuitively clear that in larger systems (with a tip scale that is not related to the channel width), finite size effects and boundary conditions become less important. We confirmed numerically that the different curves are closer to each other for a channel of twice the width. For infinitely wide channels, we expect convergence to the free growth results presented in [15].

With the phase field approach it is possible to study also transient regimes. This is for example the case for situations with collective growth of several β seeds as a ‘‘colony’’ inside the undercooled α phase. There, the inclusions grow side by side, and hence the channel geometry is effectively formed by the neighbors. Only if the fingers are sufficiently far away from each other the tips propagate independently, but then the tails can already start to interact with each other.

This situation changes when the fingers come closer to each other, such that the tips interact with each other via the diffusive and elastic fields. Therefore, we simulated dense collective growth of single crystals, and the result is shown in Fig. 3. Here, we start from the undercooled metastable α phase with four circular seeds of the β phase; notice that all of them are chosen to have the same grain orientation. Immediately after the start of the simulation the former circular seeds grow predominately along the x direction and therefore deform to ellipses (see Fig. 3a and b), since in this early regime this is for each of them the pre-

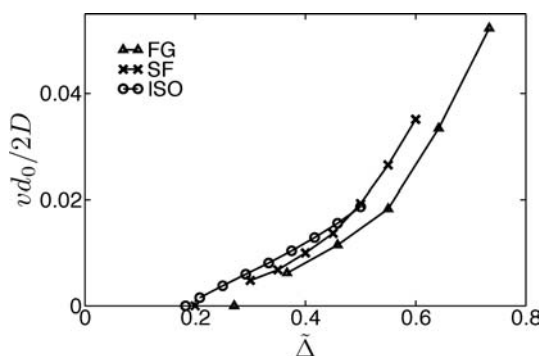


Fig. 2. Comparison of the steady state growth velocity as function of the driving force for the three different types of boundary conditions. The points of vanishing velocity match the analytical predictions for the critical driving forces. All calculations were done on a static grid with 400×1024 grid-points and the Parameters were chosen to be $\Delta_{\text{el}} = 0.05$, $\xi/W = 0.0125$.

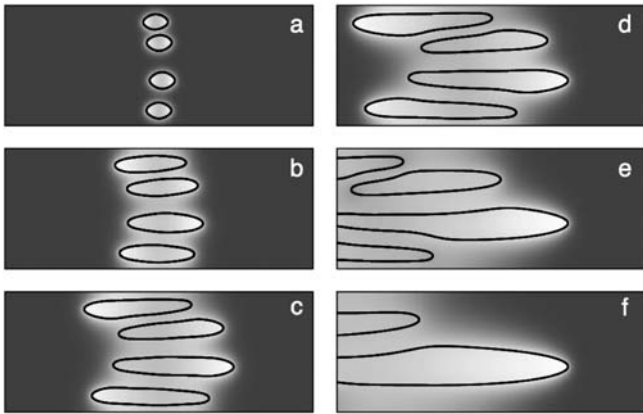


Fig. 3. Time series of collective growth of four seeds of the β phase in the undercooled α phase. The bold solid lines indicate the α/β interface, and the temperature distribution is shown by the gray scaling. From (d) on the fields are shifted to keep the most advanced interface point inside the area shown here. The System is chosen to be twice as big as for the calculations above, whereas all other parameters are the same as in Fig. 1.

ferred growth direction. As they continue to grow they start to interact with each other. Remarkably, the elastic and thermal interaction between the seeds can lead to deviations from the favored growth direction, which can be seen for example in Fig. 3c and d. Finally, one finger outgrows all the others (see Fig. 3e and f), since then the other fingers have to grow in the warm slipstream of the most advanced tip, and consequently the driving force for the phase transformation is reduced for them.

4. Plastic deformations

So far, we have taken only elastic deformations into account, assuming that the stress free eigenstrain is small, $\epsilon_{ik}^0 \ll 1$. However, in many cases this assumption is not legitimate because the structural changes or density differences can become substantial. Then the material starts to deform plastically, since the strain will also be of the order of the eigenstrain.

To go beyond the elastic limit, we started to incorporate the isotropic von Mises (or J_2) plasticity model including linear isotropic hardening. Similar to the elastic part, the model shall treat the corresponding hardening behavior, and therefore also the yield stress, as phase dependent. Due to the rate-independence of elasto-plasticity this model does not introduce a new time scale, and hence it is from a physical point of view the simplest extension. More advanced plasticity models will be investigated in a later stage.

The numerical solution of inelasticity in solid mechanics is based on the iterative solution of the discretized version of the momentum balance equations arising from discretization procedures, see e.g. [21]. Although finite elements are standard, we use finite differences along with relaxation methods here. Due to the principle of local action, the material behavior at a material point merely depends on the direct environment of this point. Therefore, the sole input for classical inelastic constitutive equations – like von Mises plasticity – is the local displacement or strain field along with history variables. Hence, the evolution equations of plastic flow are integrated on a local, material point level.

The link between the “global” boundary value problem of finding the equilibrium solution and the “local” initial value problem of inelastic stress response is the total strain tensor as derived from the unknown (nodal) displacements.

Here, we assume an additive decomposition of the total strain tensor in elastic and plastic parts, $\epsilon_{ik} = \epsilon_{ik}^e + \epsilon_{ik}^p$. The plastic part follows from time integration of the plastic evolution equations. If the yield function $f = (s_{ik}s_{ik})^{1/2} - \sqrt{2/3}y(\bar{\alpha})$ (s_{ik} is the deviatoric stress, y the current yield stress, $\bar{\alpha}$ the equivalent plastic strain) is larger or equal to zero, plastic flow commences in the considered material point and the associated flow rule $\dot{\epsilon}_{ik}^p = \gamma df/d\sigma_{ik}$ is integrated by Backward Euler. The consistency parameter γ , which also determines the evolution of equivalent plastic strain, $\dot{\bar{\alpha}} = \gamma\sqrt{2/3}$, is calculated from the consistency condition $\gamma\dot{f} = 0$ for $f = 0$. An elasto-plastic operator split leads to the radial-return method, where the stress state of the elastic predictor is corrected by a (radial) projection onto the yield surface, $f = 0$, which expands in the case of isotropic strain hardening and shifts in the case of kinematic hardening. The numerical integration of this system can be seen as a constrained optimization problem governed by discrete Karush–Kuhn–Tucker optimality conditions. We checked the validity of the implementation within the phase field framework for cyclic loading of a pure solid phase for uniaxial strain as well as simple shear and recovered the correct hysteresis.

The phase field formalism becomes relevant when we treat inhomogeneous systems, and an extreme case is a material with cracks or voids. Inside these defects the elastic constants are zero, and the interface to the solid phases is – as usual – smeared out on the scale of the phase field interface thickness. This automatically leads to traction free surfaces. A particularly useful case that we investigated more carefully is a circular hole in a two-dimensional domain, which is strained hydrostatically far away from the hole; for simplicity, we considered here only the case without hardening, hence the current yield stress equals the initial value $y = y_0$. Since the stress is concentrated around the hole with radius R , it can reach the yield limit at a larger radius with radius R_1 , depending on the applied load. Outside this circle the material response is elastic, but within the ring $R < r < R_1$ the material behavior is plastic. The analytical solution to this radially symmetric model is given in [22]. For a two-dimensional situation the nonvanishing entries of the stress tensor can be written in polar coordinates (r, φ) as

$$\sigma_{rr} = -p - s, \quad \sigma_{\varphi\varphi} = -p + s \tag{10}$$

In the elastic region, $r > R_1$, the solution is $p = -\sigma_\infty$, where σ_∞ is the remote hydrostatic pressure, and $s = y_0R_1^2/\sqrt{3}r^2$. In the plastic region $s = y_0/\sqrt{3}$ and $p = -\sigma_\infty - 2y_0 \ln(r/R_1)/\sqrt{3}$. The radius of the plastic region follows from the condition of vanishing normal stresses on the boundary of the circular hole and gives

$$R_1 = R \exp \left[\frac{1}{2} \left(\frac{\sqrt{3}\sigma_\infty}{y_0} - 1 \right) \right] \tag{11}$$

which grows exponentially with the applied stress.

For the numerical investigations, we take a quadratic system of size $L \times L$ and a circular hole in its center. At its boundaries the system is stretched orthogonally to the edges

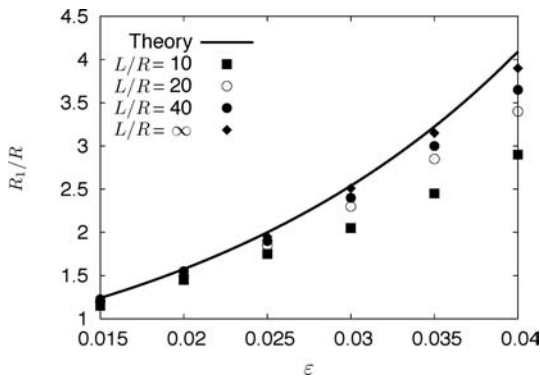


Fig. 4. Radius of the plastic region as function of the remote hydrostatic strain. The plot shows data from different System sizes, and the values extrapolated to $L/R = \infty$ are in reasonable agreement with the analytical result for an in-finitely large System.

with the same strain $\varepsilon = \sigma_{\infty}/2(\mu + \lambda)$. For a sufficiently big system, $L \gg R_1$, the results are compared to the analytical prediction. For finite system sizes, the range of the “singular” elastic field of the hole reaches the boundaries (where the displacement is kept fixed) and therefore leads to deviations; this effect is obviously larger for higher strains. Specifically, we choose a hole radius $R = 20\Delta x$ (Δx is the lattice unit) and $y_0/(\lambda + \mu) = 0.037$ and $\nu = 1/3$; system sizes vary between $L/R = 10$ to $L/R = 40$, and we use an interface thickness of $\xi/\Delta x = 2$. The results are shown in Fig. 4. In the limit of large systems they agree with the analytical prediction; remaining deviations stem mainly from the finite hole radius R/ξ , which is defined only up to $R \pm \xi$ within the phase field framework. We can therefore conclude that the plastic behavior is captured correctly.

As the next step the coupling of the elasto-plastic stress fields to the phase field dynamics will be incorporated, which should lead to a qualitatively new behavior if the stresses reach the order of the yield stress. Based on these results using von Mises plasticity as a “prototype” for an inelastic model, more advanced constitutive models will be considered, which account for effects neglected so far, such as the anisotropy of plastic flow [23], especially at finite deformations [24], or dependencies of plasticity on pressure, size or temperature [25].

5. Summary

We investigated the influence of elastic effects on the kinetics of solid-state transformations. The model, which is closely related to a sharp interface description, is applied to growth in a channel geometry. The growth velocity, in particular, depends on the specific boundary conditions for the elastic and thermal fields. In more complex situations, many seeds of the equilibrium phase lead to competitive growth situations. Finally, we discussed extensions of the present model to the incorporation of plastic effects, which are relevant for high misfit stresses.

RS and BE acknowledge financial support through ThyssenKrupp AG, Bayer MaterialScience AG, Salzgitter Mannesmann Forschung GmbH, Robert Bosch GmbH, Benteler Stahl/Rohr GmbH, Bayer Technology Services GmbH and the state of North-Rhine Westphalia as well as the European Commission in the framework of the European Regional Development Fund (ERDF).

References

- [1] A.G. Khachaturyan: Theory of Structural Transformation in Solids, Wiley, New York (1983).
- [2] A.L. Roitburd: Sov. Phys. Usp. 17 (1974) 326. DOI:10.1070/PU1974v017n03ABEH004134
- [3] M. Asta, C. Beckermann, A. Karma, W. Kurz, R. Napolitano, M. Plapp, G. Purdy, M. Rappaz, R. Trivedi: Acta Mater. 57 (2009) 941. DOI:10.1016/j.actamat.2008.10.020
- [4] R. Kupferman, D.A. Kessler, E. Ben-Jacob: Physica (Amsterdam) 231A (1995) 451.
- [5] E.A. Brener, V.I. Mel'nikov: Adv. Phys. 40 (1991) 53. DOI:10.1080/00018739100101472
- [6] D. Pilipenko, E.A. Brener, C. Hüter: Phys. Rev. E 78 (2008) 060603. DOI:10.1103/PhysRevE.78.060603
- [7] L.Q. Chen: Annu. Rev. Mater. Res. 32 (2002) 113. DOI:10.1146/annurev.matsci.32.112001.132041
- [8] W.J. Boettinger, J.A. Warren, C. Beckermann, A. Karma: Annu. Rev. Mater. Res. 32 (2002) 163. DOI:10.1146/annurev.matsci.32.101901.155803
- [9] I. Steinbach: Modelling Sim. Mater. Sci. Eng. 17 (2009) 073001. DOI:10.1088/0965-0393/17/7/073001
- [10] Y.H. Wen, Y. Wang L.Q. Chen: Acta Mater. 47 (1999) 4375.
- [11] Y.H. Wen, Y. Wang L.Q. Chen: Acta Mater. 48 (1999) 4125.
- [12] Y.H. Wen, Y.Z. Wang, L.Q. Chen: Philos. Mag. A 80 (2000) 1967. DOI:10.1080/01418610008212146
- [13] Y.H. Wen, Y. Wang L.Q. Chen: Acta Mater. 49 (2001) 13.
- [14] M. Greenwood, J.J. Hoyt, N. Provatas: Acta Mater. 57 (2009) 941. DOI:10.1016/j.actamat.2009.01.020
- [15] M. Fleck, C. Hüter, D. Pilipenko, R. Spatschek, E.A. Brener: accepted for publication in Philos. Mag. (2009).
- [16] E.A. Brener, G. Boussinot, C. Hüter, M. Fleck, D. Pilipenko, R. Spatschek, D.E. Temkin: J. Phys.—Condens Matter 21 (2009) 464106. DOI:10.1088/0953-8984/21/46/464106
- [17] E.A. Brener, V.I. Marchenko, R. Spatschek: Phys. Rev. E 75 (2007) 041604. DOI:10.1103/PhysRevE.75.041604
- [18] R. Spatschek, M. Fleck: Phil. Mag. Lett. 87 (2007) 909. DOI:10.1080/09500830701416618
- [19] C. Gugenberger, R. Spatschek, K. Kassner: Phys. Rev. E 78 (2008) 016703. DOI:10.1103/PhysRevE.78.016703
- [20] J. Slutsker, K. Thornton, A.L. Roytburd, J.A. Warren, G.B. McFadden: Phys. Rev. B 74 (2006) 914103. DOI:10.1103/PhysRevB.74.014103
- [21] J.C. Simó, in: P.G. Ciarlet, J.L. Lions (Ed.), Handbook of Numerical Analysis, Vol. 6, Elsevier Science Publisher BV (1998) 183.
- [22] J.S. Langer, A.E. Lobkovsky: Phys. Rev. E 60 (1999) 6978. DOI:10.1103/PhysRevE.60.6978
- [23] B. Eidel, F. Gruttman: Comput. Mater. Sci. 28 (2003) 732. DOI:10.1016/j.commatsci.2003.08.027
- [24] A. Bertram: Elasticity and Plasticity of Large Deformations, Springer (2005).
- [25] G.A. Maugin: The Thermomechanics of Plasticity and Fracture, Cambridge University Press (1992).

(Received October 11, 2009; accepted November 22, 2009)

Bibliography

DOI 10.3139/146.110295
Int. J. Mat. Res. (formerly Z. Metallkd.)
101 (2010) 4; page 462–466
© Carl Hanser Verlag GmbH & Co. KG
ISSN 1862-5282

Correspondence address

Michael Fleck
IFF-3, Forschungszentrum Jülich
Wilhelm-Johnen-Straße, 52425 Jülich, Germany
Tel.: +49 024 6161 4399
Fax: +49 024 6161 2620
E-mail: m.fleck@fz-juelich.de

You will find the article and additional material by entering the document number **MK110295** on our website at www.ijmr.de